Polymer Journal (2022) 54:1191–1201
https://doi.org/10.1038/s41428-022-00667-3

ORIGINAL ARTICLE

# Tetrazine-based 1D polymers for the selective chemiresistive sensing of nitrogen dioxide via the interplay between hydrogen bonding and n-heteroatom interactions

Aswani Raj K[1] · Guruprasad Gorthala[2] · Ruma Ghosh[2] · Rajeswara Rao Malakalapalli[1]

Received: 3 February 2022 / Revised: 4 May 2022 / Accepted: 6 May 2022 / Published online: 11 July 2022


## Abstract

There is a great demand for the reliable and quantitative detection of $NO_2$ to monitor and control environmental pollution and subsequently prevent harmful human health effects. Metal oxide-based chemiresistive sensors detect this notorious gas, but high operating temperatures (100–500 °C) limit their applicability. Organic polymers can perform room-temperature sensing, but such sensors are rare due to the lack of functional groups needed for effective analyte detection and discrimination. This paper describes the selective sensing of $NO_2$ gas by incorporating well-defined N-heteroatom functionalization into organic polymers. Three structurally analogous novel one-dimensional tetrazine polymers (*p*-phenyl-, *m*-phenyl- and thienyl-substituted) were synthesized in this study. Incorporating such π units allows the polymers to be stabilized in their partially oxidized forms, resulting in various ratios of dihydrotetrazine (0–55%):tetrazine units in the polymer backbone. All of the synthesized polymers were tested as resistive sensors for $NO_2$. The polymer *p*PTz, possessing the highest dihydrotetrazine (~55%) content, exhibited the best performance for detecting 25–150 ppm $NO_2$ compared to the other two polymers (*m*PTz, TTz). The *p*PTz-based sensor was found to be fast, taking 115 s to respond to 150 ppm $NO_2$, reversible with a recovery time of 560 s for 150 ppm $NO_2$ and could sense $NO_2$ at room temperature. *p*PTz was also found to be highly selective for $NO_2$ over the other tested analytes, such as $NH_3$, EtOH, MeOH, acetone, 2-nitro toluene, and humidity. Synergetic interactions arising from –NH hydrogen bonding (dihydrotetrazine) and the N-heteroatom (tetrazine) functionalities in *p*PTz were expected to be the reason for the superior and selective detection of $NO_2$. The structure-property relationship studies reported in this work may pave the way for designing functional conducting polymers for excellent chemiresistive sensing.

## Introduction

Nitrogen dioxide ($NO_2$) is a hazardous oxidizing gas that is primarily emitted from the combustion of fossil fuels in motor vehicles, industries, power plants, etc [1]. It poses serious health risks by causing damage to the lungs, upper respiratory tract and cardiovascular system [1, 2]. In addition, it also has detrimental effects on the environment because it is a significant cause of acid rain and photochemical smog [3, 4]. Thus, it is imperative to develop efficient techniques for the real-time sensing of this notorious gas for the sake of human safety, protection and proper environmental monitoring. Many gas sensing methods, such as colorimetric [5, 6], conductometric [7], potentiometric [8], chemiresistive [9] and organic field-effect transistor-based (OFET) [10, 11] methods, have been employed to detect this vapor. Among these, chemiresistive sensors, which measure the change in resistance of the sensing materials when exposed to an analyte, have attracted much attention due to their simple operating principle, compact but straightforward device structure, low cost, and low power requirements [12]. Resistive sensors can also be integrated with complementary metal-oxide-semiconductor

These authors contributed equally: Aswani Raj K, Guruprasad Gorthala

**Supplementary information** The online version contains supplementary material available at https://doi.org/10.1038/s41428-022-00667-3.

✉ Rajeswara Rao Malakalapalli
rajesh@iitdh.ac.in

[1] Department of Chemistry, IIT Dharwad, Dharwad, Karnataka 580011, India

[2] Department of Electrical Engineering, IIT Dharwad, Dharwad, Karnataka 580011, India

(CMOS) platforms that offer vast opportunities for miniaturization and portability [13, 14]. The critical component in a resistive sensor is the sensing layer, which significantly influences the sensing ability of the sensor. Thus, employing the appropriate materials is necessary for achieving superior and selective sensing. In pursuit of such sensing layers, several materials have been designed and explored over the last few decades. Metal oxides are one of the most widely studied sensing materials. These semiconductor-based chemiresistive sensors have also been tested for $NO_2$ and were found to be highly sensitive for this environmental pollutant [15–17]. Unfortunately, these materials primarily operate at only high temperatures (100–500 °C), which leads to increased power consumption [15, 16]. Recently, many efforts have been made to discover sensing materials that can sense gases at room temperature [18, 19].

In addition, as a specific interest, organic π-conjugated materials such as carbon nanomaterials [20] and one-dimensional (1D) organic semiconducting polymers [21, 22] have been widely investigated as chemiresistive gas sensing materials due to their easy synthesis procedures, low cost, high sensitivity, flexibility and room temperature operation. The 1D conducting polymers that have been explored for sensing include polyaniline (PANI) [22, 23], poly(3,4-ethylene dioxythiophene) (PEDOT) [24], polythiophenes (PThs) [21], polypyrroles (PPys) [25], etc. The sensors developed by these polymeric sensing layers exhibited promising results for a wide range of analytes; however, their sensitivities and selectivities are inferior to those of metal oxides, possibly due to a lack of adequate coordinating/interacting sites for the analytes in the polymeric backbone. However, one molecular design strategy that has been successfully demonstrated to improve the sensitivity and selectivity of sensors (optical and fluorescent sensors, etc.) [26, 27] in general is to attach coordinating/functional groups to the polymeric backbone to induce strong interactions with the analyte(s). Along this line, chemiresistive sensors based on functionalized organic polymers, polymer/graphene oxide, and polymer/carbon nanotubes have been developed with improved selective sensing of various analytes [28–33]. However, the number of examples reported is extremely scarce. Moreover, to the best of our knowledge, coordinating unit integrated organic 1D polymers have never been tested for chemiresistive sensing. It is worth noting that coordinating unit-embedded porous organic polymers (two-dimensional polymers), such as covalent triazine frameworks (CTFs) [34, 35], covalent organic nanosheets (CONs) [36], graphitic carbon nitride (g-$C_3N_4$) [37], heptazine-based organic frameworks [38], and imine-linked covalent organic frameworks (COFs) [39], have exhibited improved sensing performance toward various analytes, although they are not very relevant in the context of conducting 1D polymers. Because of the ease of synthesis and the ability to effectively propagate π delocalization, 1D polymers are expected to have a distinct advantage over porous organic polymers for sensing applications.

In this work, we designed and developed three new 1D polymers consisting of nitrogen atom-loaded tetrazines as sensing layers for the chemiresistive sensing of $NO_2$. The structural, optical and electronic properties of the polymers were found to be significantly different from each other as the aryl units (from *p*-phenylene to *m*-phenylene and thienyl) varied between the tetrazine units. Most importantly, the aromatic units allowed the tetrazine polymers to stabilize in varying proportions of (unoxidized) dihydrotetrazines (55% to 0) and (oxidized) tetrazine units. All three tetrazine-based polymers were thoroughly tested for their capabilities to detect different concentrations of $NO_2$ ranging from 25 to 150 ppm at ambient temperature. One of the three polymers was discovered to have the best performance toward $NO_2$. These polymers were also assessed for their selectivities towards the obnoxious gas by exposing them to different gases present in the environment, such as $NH_3$, humidity and a few other volatile organic compounds (VOCs). The detailed results are presented and discussed in the subsequent sections.

## Experimental section

### Material synthesis

Synthesis of tetrazine polymers: Aryl dicarbonitrile (1.56 mmol, 1 eq), sulfur powder (6.24 mmol, 4 eq) and 75% hydrazine hydrate (15.6 mmol, 10 eq) in ethanol were refluxed for three days. The reaction mixture was then concentrated under reduced pressure, and the crude product was used in the next step without further purification.

The crude product was suspended in an acetic acid/water (2:1) solution of $NaNO_2$ (7.6 mmol, 5 eq) under ice-cold conditions and stirred at room temperature for two days. Next, the solid was collected by vacuum filtration and washed with hot DMF, water, methanol and acetone and by Soxhlet extraction in toluene and ethanol for 2 and 1 days, respectively, to remove the sulfur and oligomeric units. Finally, the solid was vacuum-dried for two days.

#### Poly[(1,4-phenylene)-*alt*-(3,6-(1,2,4,5-tetrazine)/3,6-(1,2,4,5-dihydrotetrazine))] (*p*PTz)

Reddish-brown solid, yield: 76%; $^{13}C$ cross-polarization magic-angle-spinning ($^{13}C$ CPMAS) NMR (100 MHz, δ in ppm) 120-140, 162, 167; IR (KBr pellet): $\nu_{max} = 1604, 1450, 1390\ cm^{-1}$; UV–Vis-NIR (powder): red edge – 645 nm (band gap – 1.92 eV).

#### Poly[(1,3-phenylene)-*alt*-(3,6-(1,2,4,5-tetrazine)/3,6-(1,2,4,5-dihydrotetrazine))] (*m*PTz)

Pink solid, yield: 30%; $^{13}$C CPMAS NMR (100 MHz, δ in ppm): 121-140, 163, 166.8; IR (KBr pellet): $\nu_{max} = 1603$, 1455, 1373 $cm^{-1}$; UV–Vis-NIR (powder): red edge – 642 nm (bandgap – 1.93 eV). The low yield from this reaction can be attributed to the steric factors caused by 1,3-substitution.

#### Poly[(2,5-thiophene)-*alt*-(3,6-(1,2,4,5-tetrazine))] (TTz)

Dark red solid, yield: 80%; $^{13}$C CPMAS NMR (100 MHz, δ in ppm): 21-146, 161.4; IR (KBr pellet): $\nu_{max} = 1601$, 1453, 1384 $cm^{-1}$; UV–Vis-NIR (powder): red edge – 714 nm (band gap – 1.73 eV).

#### Synthesis of Model Compound: 3,6-di(thiophen-2-yl) −1,2,4,5-tetrazine (MTTz) [40]

To a dry round-bottom flask was added thiophene-2-carbonitrile (100 mg, 0.75 mmol), sulfur powder (47.8 mg, 1.49 mmol), 75% hydrazine monohydrate (3.72 mmol, 5 eq) and ethanol (15 ml). The mixture was refluxed at 80 °C for two hours and cooled to room temperature. The red precipitate was collected *via* filtration and thoroughly dried under vacuum. It was used directly for the next step of oxidation without further purification.

The red precipitate was added to a round bottom flask followed by isoamyl nitrite (5 ml) and chloroform (10 ml). The mixture was stirred at room temperature for 12 h. The solvent was then removed by rotary evaporation, and the collected residue was subjected to silica gel column chromatography to afford the target molecule as red crystals in 55% yield (125 mg). $^{1}$H NMR (400 MHz, $CDCl_3$, δ in ppm): 8.28-8.27 (m, 2H), 7.69-7.67 (m, 2H), 7.28-7.26 (m, 2H); $^{13}$C NMR (400 MHz, $CDCl_3$, δ in ppm): 161.6, 136, 132.6, 131.0, 129.1; UV–Vis ($CHCl_3$ solution): red edge – 424 nm.

#### Electrode fabrication

For electrochemical measurements, the insoluble **pPTz** polymer was coated on a glassy carbon electrode using the following procedure. First, the electrode was thoroughly washed with water and dried in air. Later, **pPTz** (5 mg; 75%), Nafion binder (1 mg; 20%), and carbon black (0.66 mg) were mixed in ethylene glycol (500 µl) and stirred for 12 hr to generate a homogenous solution. In the next step, 0.5 µl of the solution was drop-casted on the glassy carbon electrode, and the electrode was dried under vacuum for 6 h.

### Material characterization

An Agilent Cary 5000 UV-Vis-NIR spectrophotometer was employed to study the optical properties of the synthesized polymers. The NMR spectra for the polymer structural characterizations were obtained on a JEOL Resonance ECZ-400R spectrometer. Infrared spectra were recorded on a Nicolet Impact-400 FTIR spectrometer. Solid samples were recorded as KBr wafers and analyzed. Morphological studies of the sensing materials were carried out using field emission scanning electron microscopy (FESEM; Carl Zeiss Gemini-300). Thermogravimetric analysis (TGA) was carried out on an SDT Q600, TA Instruments, USA. Cyclic voltammetry studies were performed on a CHI instrument (model no: 660E). Density Functional Theory (DFT) calculations of the molecular structures (in the gas phase) and the molecular orbital energies were carried out at the B3LYP/6-31 G(d) level as implemented in Gaussian 16. The figures were generated with GaussView 6.0.

### Gas sensing setup and measurements

The synthesized polymer samples were dispersed in ethanol and coated on interdigitated electrodes (IDEs) by drop-casting the former on the latter and dried until the solvent was evaporated. Then, the polymer-coated IDEs were probed inside an airtight stainless-steel chamber. The test chamber was connected to a data acquisition unit (Keithley 6510 data acquisition (DAQ)), which facilitated continuous recording the sensing layer's resistance at a time interval of 1 s. The gas inlet of the stainless steel chamber was connected to a gas mixer that received input from multiple mass flow controllers (MFCs). This study required two MFCs—one of the MFCs, MFC1, was utilized to flow the calibration gas, which was dry air in our case; the other MFC, MFC2, was used to introduce the target gases. After the sensor devices were mounted inside the test chamber, the chamber was evacuated before conducting any experiments to avoid contamination. Then, the sensors were purged with dry air at a flow rate of 100 standard cubic centimeters per minute (sccm) for one hour to stabilize the baseline resistance of the sensing layer. Next, different concentrations of the target gases $NO_2$, $NH_3$, 2-NT, ethanol, methanol, acetone, and $H_2O$ were introduced into the test chamber by varying the ratios of the flow rates MFC1 and MFC2. The sensors were exposed to a particular gas concentration for 5 min, followed by 10 min of purge with the calibration gas.

## Results and discussion

The tetrazine-based polymeric sensing materials, 1,4-phenylene tetrazine (***p*PTz**) [41], 1,3-phenylene tetrazine

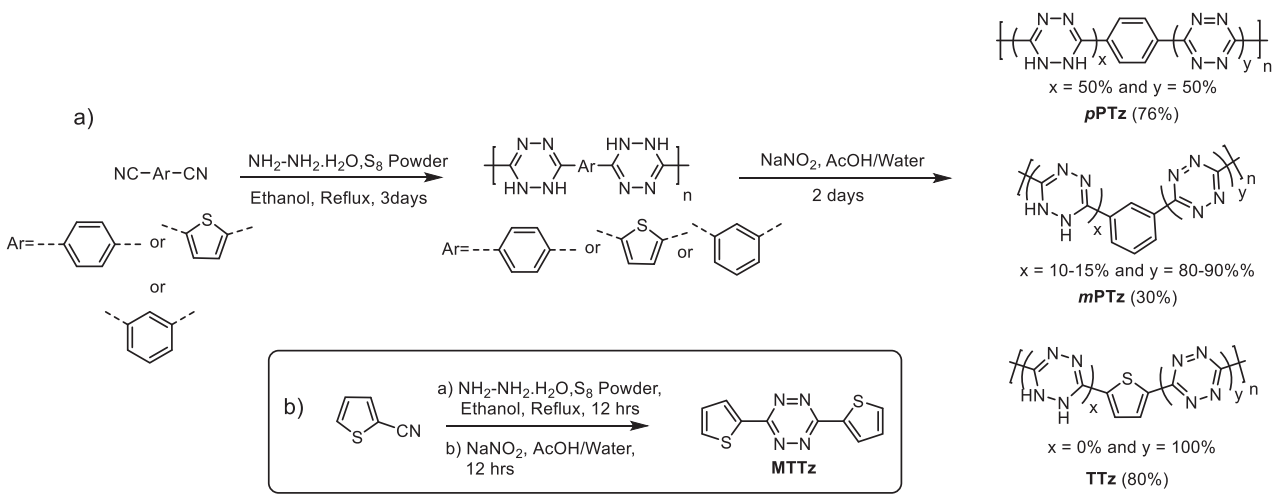


**Scheme 1** Synthesis of polymers ***p*PTz**, ***m*PTz** and **TTz** and the model compound **MTTz**

(***m*PTz**) and thiophene tetrazine (**TTz**) polymers, were synthesized (Scheme 1) in two steps by using Pinner synthetic protocols using aryl dicarbonitriles (1,4-dicyanobenzene, 1,3-dicyanobenzene and 2,5-dicyanothiophene, respectively). The appropriate aryl dicarbonitrile was reacted with hydrazine hydrate (75%) and sulfur in ethanol for three days to achieve the unoxidized dihydrotetrazine polymers. The intermediates were then oxidized using aqueous sodium nitrite for 48 h to generate the tetrazine polymers. The resulting intensely colored solids (pink to reddish-brown) were filtered and purified with hot DMF and by Soxhlet extraction (toluene and ethanol over 24 h). The thermal stability of the polymers was evaluated by TGA, which showed that the decomposition temperatures of these polymers were above 250 °C (Fig. S1).

The successful preparation of the polymers was verified by Fourier transform infrared (FT-IR) spectroscopy and $^{13}$C CP-MAS NMR spectroscopy. The appearance of characteristic tetrazine signals corresponding to -C = N- and -N-N- at ~1603 $cm^{-1}$ and ~1380 $cm^{-1}$, respectively, along with the other customary signals of -C = C- and -C-H at ~1453 $cm^{-1}$ and ~2920 $cm^{-1}$, confirmed the formation of the polymers (Fig. 1a). On the other hand, the $^{13}$C CP-MAS NMR spectrum of the polymers displays a tetrazine carbon (-C = N-) signal at ~162 ppm, again confirming the formation of the polymers. The weak signal at ~115 ppm corresponds to the end-group nitrile (-C ≡ N) and is indicative of the presence of a long polymeric chain. For all the polymer phenylene/thienyl groups, carbon signals appeared between 120 and 140 ppm (Fig. 1b). The $^{13}$C NMR peak pattern and the positions of the polymers were also identical to the solution soluble model compound (**MTTz**). However, ***p*PTz** and ***m*PTz** showed an additional signal (b) at ~167 ppm belonging to unoxidized dihydrotetrazine units. This indicates that the polymers were not completely oxidized during the reaction of dihydrotetrazine with aqueous sodium nitrite but instead consisted of both tetrazine and dihydrotetrazine units. Furthermore, the peak intensity of the dihydrotetrazine signal was higher for ***p*PTz** (equivalent to the signal of oxidized tetrazine) than for ***m*PTz**, but vanished completely for **TTz**. Peak deconvolution fitting of these NMR signals indicated that ***p*PTz** contains a high percentage of dihydrotetrazines (55%) compared to as little as 25% in ***m*PTz** (Fig. S2).

To understand the incomplete oxidation process of the polymers, density functional theory (DFT) calculations were carried out on model polymeric fragments that were unoxidized, partially oxidized, and oxidized (Fig. 2a). The DFT-evaluated HOMO energies indicated that among all three unoxidized and partially oxidized fragments, the thiophene congeners (–5.48 eV and –5.72 eV) possessed relatively higher HOMO energies, which provides a higher driving force for the oxidation to yield a fully oxidized material. On the other hand, the HOMOs are somewhat higher for the partially oxidized phenylene fragments (–5.92 eV), allowing the stabilization of the intermediate partially oxidized forms. Moreover, such systems also gain additional stability *via* donor-acceptor interactions between unoxidized (D) and oxidized (A) species. As depicted in Fig. 2a, the HOMOs are localized on the dihydrotetrazine units, while the LUMOs are centered around the tetrazine units. However, the variable oxidation ratios for *para*- and *meta*-phenylene systems, despite having the same HOMO energies, could be attributed to weak D-A interactions arising from cross-conjugation in the *meta*-system.

The diffuse reflectance optical properties of the solid polymers were studied using UV–Vis-NIR spectroscopy (Fig. 1c). All of the polymers displayed broad and strong absorption spectra covering most of the visible region with a red edge at ~650–725 nm. ***p*PTz** and ***m*PTz** showed dual-band features (~300 to 450 nm and ~550 nm) while this feature merged and appeared as one broad band for **TTz**. The former was ascribed to the π-π* transition, while the latter refers to the n-π* transition originating from tetrazine

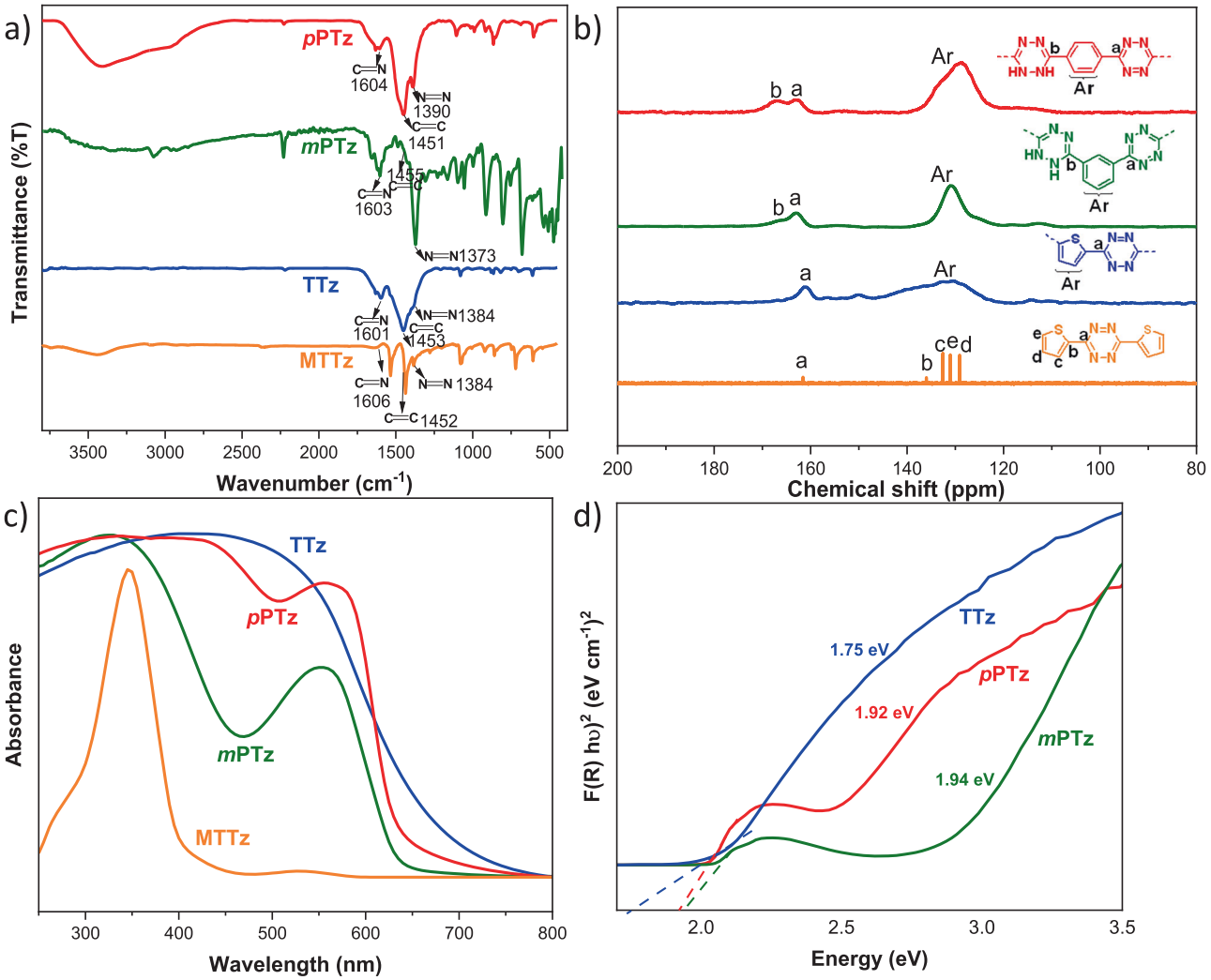


**Fig. 1** Overlay of (**a**) FT-IR, (**b**) $^{13}C$ CP-MAS NMR, (**c**) diffuse-reflectance UV–Vis absorption spectra and (**d**) Kubelka-Munk spectra of ***p*PTz**, ***m*PTz**, **TTz** and the model compound **MTTz**. The absorption spectrum of **MTTz** was measured in a dilute $CHCl_3$ solution ($1 \times 10^{-5}$ M)

units. The optical band gaps calculated from the onset absorption of the polymers (***p*PTz**, ***m*PTz** and **TTz**) were 1.92, 1.94, and 1.75 eV, respectively (Fig. 1d). ***m*PTz** vs. ***p*PTz** showcased a higher bandgap due to the cross-conjugation arising from *meta*-connection. However, among the three, the thiophene congener (**TTz**) possessed the narrowest bandgap, which was attributed to heteroatom-assisted enhanced π-delocalization.

DFT calculations of the molecular structures of the model compounds and polymers were optimized. The optimized structures revealed a planar backbone for all three polymers due to alternating aryl and tetrazine units (Fig. 2b). However, ***p*PTz** and **TTz** possess a linear chain conformation, while ***m*PTz** has a zigzag arrangement due to the *meta* connections. The HOMOs/LUMOs of the polymers were predicted to be −5.97 eV/−2.96 eV, −6.08 eV/−2.92 eV and −6.18 eV/−3.66 eV, leading to band gaps of 3.01, 3.17 and 2.51 eV, respectively, for ***p*PTz**, ***m*PTz** and **TTz**. The observed trend in the predicted bandgaps was in line with the experimentally deduced optical bandgaps. However, the overestimation of the DFT-predicted bandgaps compared to the experimental bandgaps can be attributed to the gas phase DFT calculations. The high HOMOs and low LUMOs indicate that the polymers are electron deficient and are ideal for *p*-type chemiresistive sensing materials. To validate the HOMO and LUMO energy levels evaluated by DFT, we performed cyclic voltammetry of **pPTz**. The polymer exhibited a reduction potential at –1.39 V vs. $Fc/Fc^+$. The corresponding LUMO energy was calculated to be 3.01 eV, matching well with the DFT-deduced LUMO energy (Fig. S4). Since the polymer is electron deficient, no oxidation potential was observed within the measured solvent window (dichloromethane); thus, the HOMO and the bandgap could not be evaluated.

The morphology of the polymers was studied by FESEM (Fig. S5). The polymers showed polymeric aggregates leading to sheet/flake-like morphologies with high surface areas. This

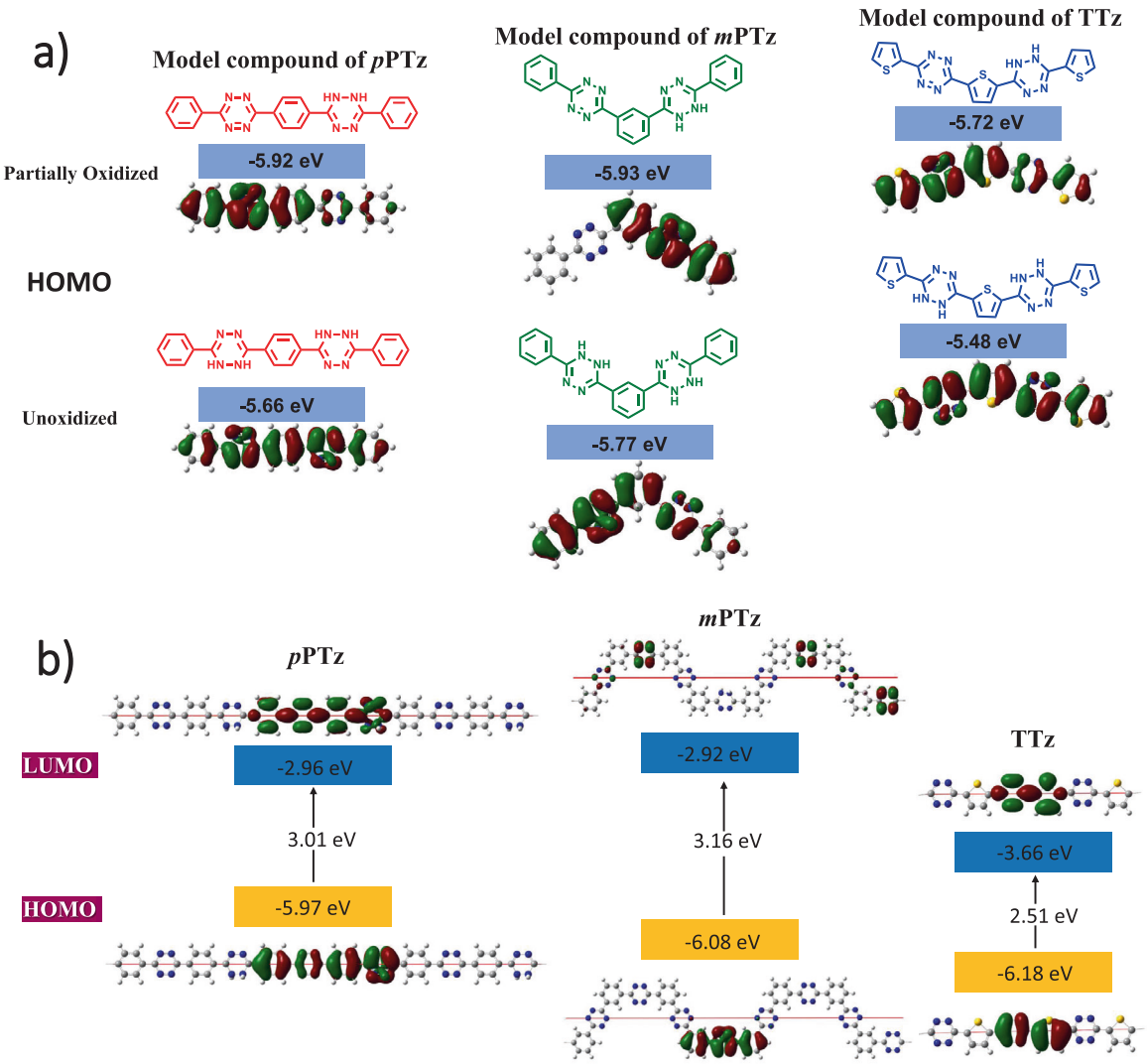


**Fig. 2** DFT-calculated HOMO energy levels and Frontier molecular orbitals plots of (**a**) representative fragments of the polymers ***p*PTz**, ***m*PTz** and **TTz** and (**b**) polymers ***p*PTz**, ***m*PTz** and **TTz**

can be attributed to the polymers' planar geometry, which allows strong intermolecular interactions.

The N-rich tetrazine polymers are expected to be suitable sensing layers for the chemiresistive sensing of various analytes. Thus, the synthesized polymers were tested against several gaseous analytes. Starting with $NO_2$, the sensing layer was exhaustively tested with four different concentrations of $NO_2$ (25–150 ppm) at 25 °C. The resistances of the sensors were observed to decrease in the presence of $NO_2$, and the response of the sensors was calculated using Formula (1).

$$Response\ (\%) = \left|\frac{R_a - R_g}{R_a}\right| \times 100 \qquad (1)$$

where $R_g$ is the resistance of the sensors in the presence of the target gas and $R_a$ is the baseline resistance.

Figure 3a shows the dynamic response of ***p*PTz** to $NO_2$ at concentrations of 25–150 ppm. The ***p*PTz** polymer's response for $NO_2$ was found to vary between 10.6% (25 ppm) and 37% (150 ppm). The response of the semiconducting polymer was found to increase almost linearly with the concentration of $NO_2$, as is evident from the inset in Fig. 3a. The adj $R^2$ value was found to be 0.96399, which expresses a good degree of fit. Due to the experimental setup limitations, the sensors could not be tested with lower concentrations of $NO_2$. That is why the limit of detection (LOD) of the developed sensor was statistically calculated following a previously reported method [42]. The LOD of the ***p*PTz**-based sensor for $NO_2$ was 5.67 ppm.

To confirm the reproducibility, we prepared four sensor devices and tested them with 25–150 ppm $NO_2$. The standard deviation for the four sensor devices was calculated and plotted, as shown in Fig. 3b. The deviation in the response of the sensors was found to be a maximum of 2.95% for 150 ppm $NO_2$, whereas it was the lowest (1.05%) in the case of 25 ppm $NO_2$. Along with the response and reproducibility, other

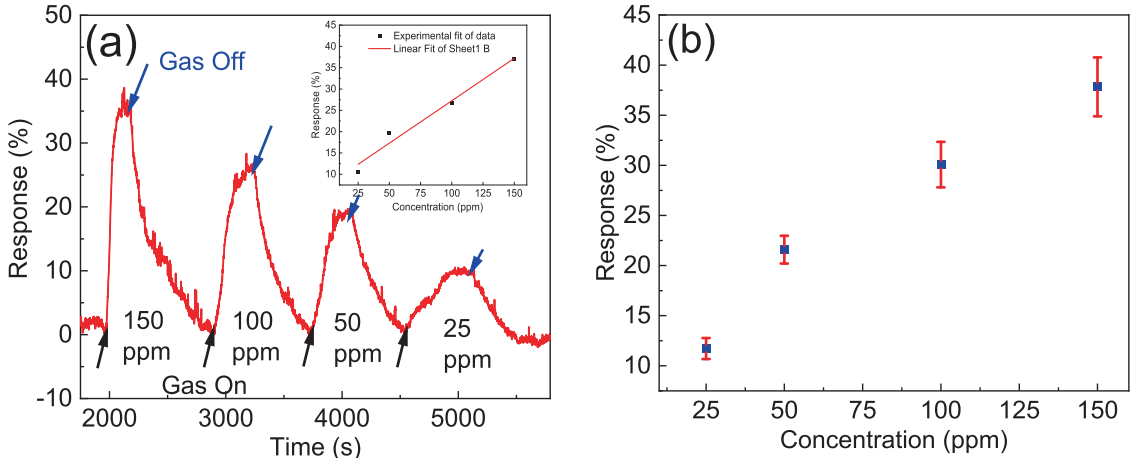


**Fig. 3** **a** Response of the ***p*PTz** polymer to different concentrations of $NO_2$ at room temperature (25 °C). The inset shows the linear fitted graph of the concentration *vs*. response. **b** Variations in the responses of the four different sensor devices for 25–150 ppm $NO_2$

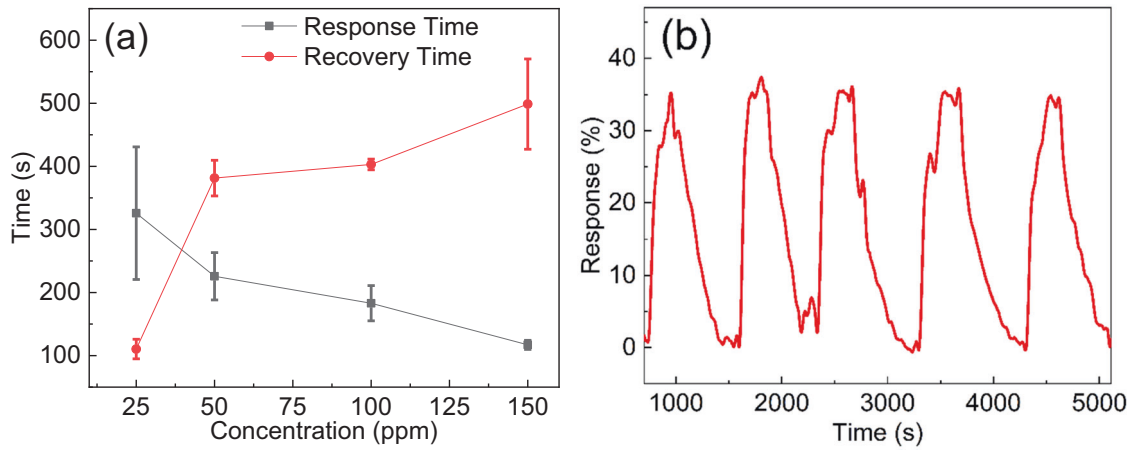


**Fig. 4** **a** Response times and recovery times of the four devices developed with ***p*PTz** for different concentrations of $NO_2$. (**b**) Repeatability test results of the ***p*PTz**-based sensor to 150 ppm $NO_2$

essential attributes of gas sensors are the response times and recovery times. A resistive vapor sensor's response time ($\tau_{res}$) is the time required to attain 90% of the steady-state response for a particular vapor concentration. The recovery time ($\tau_{rec}$) is defined as the time taken by the sensor to recover to 10% of the baseline resistance after the target gas is removed from the proximity of the sensor. The response times and recovery times of four different devices developed with ***p*PTz** for different concentrations of $NO_2$ were calculated and are shown in Fig. 4a. The $\tau_{res}$ was observed to get shorter with an increase in the concentration of $NO_2$ and was found to be 428 s for 25 ppm $NO_2$, which was reduced to 115 s when the concentration of the gas was increased to 150 ppm. This result perhaps occurred because as the concentration of $NO_2$ increased, more number of gas molecules were present in the proximity of the sensing material for reaction, thereby expediting electronic exchanges. However, the opposite trend was observed in the case of recovery time. The $\tau_{rec}$ was calculated to be 94 s for 25 ppm of the target analyte, but the recovery time increased to 560 s while attempting to recover the sensor after exposing it to 150 ppm $NO_2$.

The slower recovery with increasing concentration of $NO_2$ can be attributed to more desorption of gas molecules from the material's surface that happens after the exposure. More variations in response time were found in the case of 25 ppm of $NO_2$ with a standard deviation of 105 s, and the deviation was lowest (7.2 s) in the case of 150 ppm $NO_2$. However, in the case of recovery time, the maximum deviation of 71.6 s was found for 150 ppm analyte, and the lowest variation of 8.5 s was observed for 100 ppm. The variations in the response, response times and recovery times across the devices could be attributed to multiple factors, including the variation in the number of layers coated on the electrodes and the extent of the overlap between the polymer layers.

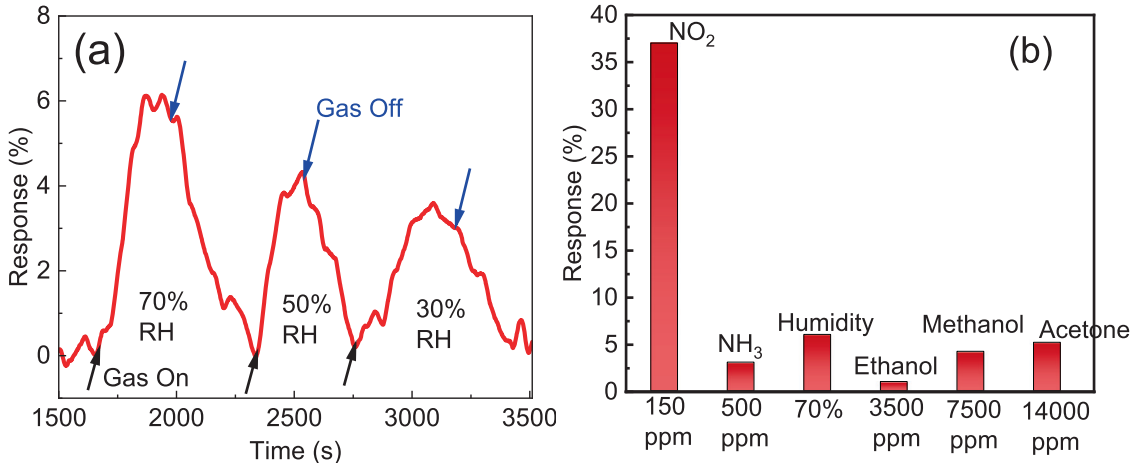


**Fig. 5** **a** Response of the ***p*PTz** polymer to different RH values. **b** Selectivity test results of the ***p*PTz** sensor

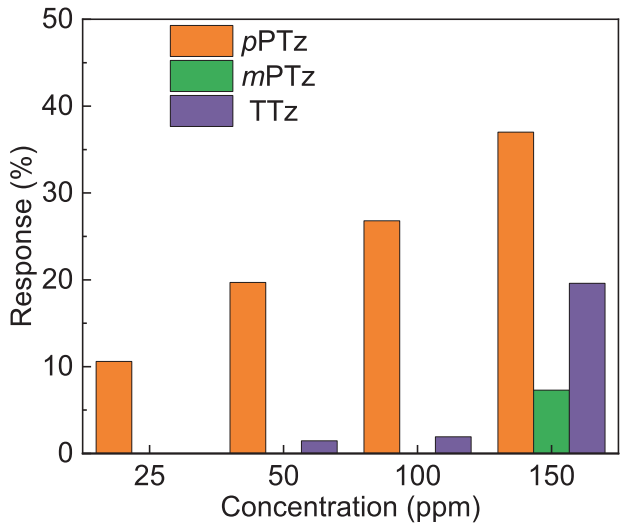


**Fig. 6** Response of ***p*PTz**, ***m*PTz**, and **TTz** polymers to 25–150 ppm $NO_2$

It is equally important to ascertain whether the sensor's response repeats if exposed to the same concentration of the target gas multiple times. Hence, the ***p*PTz**-based sensor was exposed to five cycles of $NO_2$ (150 ppm) at room temperature, and the results were found to be highly repeatable with a maximum variation of ~3% of the response (Fig. 4b).

The primary advantage of a gas sensor that works at room temperature is reduced power consumption, which eliminates heating elements from the sensor devices and the accessories required to maintain and monitor the required temperature. However, the performance of room temperature operable sensors is expected to be affected by humidity. Hence, evaluating the response of the gas sensor in the presence of moisture is very important. The ***p*PTz**-based sensor was exposed to 30%, 50%, and 70% RH, and the response was found to be 4%, 4.8%, and 6.6%, respectively, as shown in Fig. 5a. This response is much lower than the sensor's response to $NO_2$. In addition to humidity, the developed sensor was tested against five more vapors, including pollutants such as $NH_3$, and gases that are present in the environment such as 2-nitrotoluene (2-NT) and certain volatile organic compounds including ethanol, methanol and acetone. ***p*PTz** showed absolutely no response toward 2-NT at any concentration tested (up to 200 ppm), and hence, Fig. 5b does not represent any response corresponding to 2-NT. For the other compounds, an observable response was achieved at only very high concentrations. For example, $NH_3$ exhibited a detectable response only after the concentration reached 500 ppm (Fig. 5b), which was also found to be very low (~3% for 500 ppm $NH_3$). Similarly, for ethanol, methanol and acetone, a detectable response was observed at 3500 ppm, 7500 ppm and 14,000 ppm, respectively, which was also very low compared to the response observed for $NO_2$. Hence, ***p*PTz** was found to be highly selective for $NO_2$.

A rapid decrease in the sensor's resistance in the presence of $NO_2$ and its return to the initial stage upon venting the analyte gas indicates that the sensor has *p*-type semiconducting behavior. Typically, the oxidizing $NO_2$ upon its adsorption onto the surface of the sensing layer annihilates the electrons from the surface of the sensing layer and accumulates more holes. As a result, the concentration of the holes on the surface of the sensing layer increases, and thus, the resistance of the *p*-type sensor decreases.

In addition to the ***p*PTz** polymer, we also tested the ***m*PTz** and **TTz** polymers. These sensing layers were tested with 25–150 ppm of $NO_2$. Among the three, ***p*PTz** exhibited the best response, as is evident from Fig. 6. No change in the resistance was observed in the ***m*PTz** sample until it was exposed to 150 ppm of the pollutant. Similarly, the response of **TTz** (~18% to 150 ppm $NO_2$) was also found to be lower than the response exhibited by ***p*PTz**.

The rationale behind the high selectivity of ***p*PTz** toward $NO_2$ over other analytes ($NH_3$, ethanol, methanol, acetone,

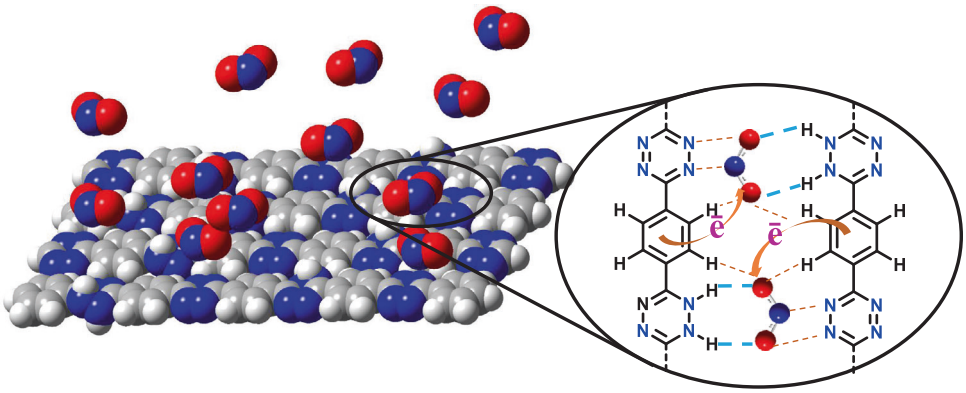

**Fig. 7** Schematic representation of the interaction of ***p*PTz** with $NO_2$

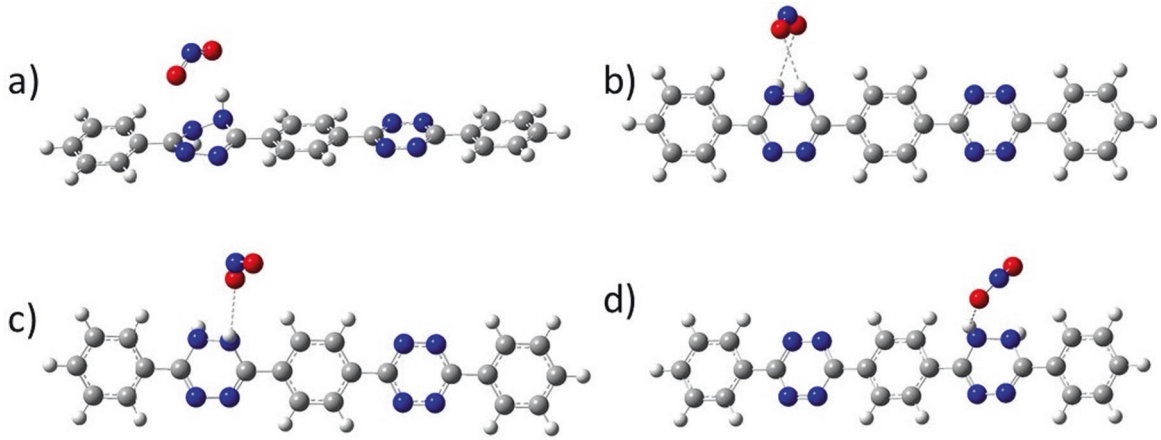


**Fig. 8** Different modes of interaction between $NO_2$ and the partially oxidized model compound. The calculated bandgap variations between the free system and the adduct were (**a**) 1.2%, (**b**) 2.5%, (**c**) 2.6%, and (**d**) 7.9%

2-NT and water) and the superior performance of ***p*PTz** over the other sensors (***m*PTz** and **TTz**) can be attributed to the unique structural arrangement associated with this polymer. The presence of both tetrazine units (~50%) and dihydrotetrazine units (~50%) in ***p*PTz** induces N-heteroatom (tetrazine) and hydrogen bonding (dihydrotetrazine) interactions with $NO_2$ (Fig. 7a), which promotes efficient adsorption of the analyte onto the polymer surface and subsequently leads to superior sensing performance. However, such hydrogen bonding interactions may not be feasible for other tested analytes. Similarly, ***m*PTz** and **TTz** cannot induce hydrogen bonding interactions with $NO_2$ due to the low concentration or absence of the dihydrotetrazine units. The presence of tetrazine units is also crucial, as they play a critical role in conducting properties and for effective analyte binding. To show the role of tetrazine units in the polymeric backbone, we employed a tetrazine-free polymer. fully dihydrotetrazine-loaded polymer (**U*p*PTz**) for $NO_2$ sensing (Fig. S6). It was found to exhibit much lower performance (~14% response toward 150 ppm $NO_2$) than what was demonstrated by ***p*PTz**. This indicates that dihydrotetrazine and tetrazine moieties are key to inducing the synergetic interactions of H-bonding and N-heteroatom interactions (and enhancing the polymer conducting properties) for the binding of $NO_2$ onto the sensing layer, thereby leading to superior sensing.

To understand the interactions between $NO_2$ and the dihydrotetrazine units, DFT calculations were used to optimize the different modes of the interactions and evaluate the critical parameters such as adsorption energy ($E_{ads}$) and the average energy gap variation ($E_g^a$). As Fig. 8 depicts, $NO_2$ interacts with NH and N atoms (mode a); two NH atoms (mode b); one NH atom (outward $NO_2$ orientation, mode c); and one NH atom (inward $NO_2$ orientation, mode d) of the dihydrotetrazine unit. In the optimized structures, the minimum distance between the tetrazine units and $NO_2$ is ~2.50 Å, which is well within the secondary bonding interactions (physisorption), and the negative $E_{ads}$ values (~5 kJ/mol) indicate that the analyte-compound interactions are stable. Typically, when an analyte interacts with a sensing layer, there is a considerable influence on the energy levels (bandgap) of the material; as a result, the resistance of the material

will vary, and the stronger the interactions are, the higher the bandgap variation between the host layer and the analyte adsorbed host layer will be. The bandgap variations ($E_g^a$ values) for the modes of interactions a-d were calculated to be 1.2%, 2.5%, 2.6% and 7.9%, respectively (Fig. 8). The electronic energy levels of the tetrazine compound were greatly affected when $NO_2$ interacted with one NH moiety of the dihydrotetrazine unit in an inward orientation. Such an orientation allows $NO_2$ to develop multiple interactions with the neighboring tetrazine units.

## Conclusions

We developed three new N-heteroatom functionalized tetrazine-based polymers for the selective sensing of $NO_2$ gas. The polymers exhibited deep colors and narrow optical bandgaps (1.7–1.9 eV), indicating that they are suitable for semiconducting applications. All of the polymers were tested with different concentrations of $NO_2$ at room temperature. Among the three, ***p*PTz** was found to exhibit the highest response to $NO_2$ in the concentration range from 25 to 150 ppm. The response ranged from 10.6% for 25 ppm to 37% for 150 ppm $NO_2$. Furthermore, this novel polymer exhibits a fast response, recovery properties, and excellent repeatability at room temperature. Moreover, ***p*PTz** vs. ***m*PTz** and **TTz** demonstrated superior sensing ability due to the tetrazine and dihydrotetrazine units in the polymeric backbone, enabling strong N-heteroatom and hydrogen bonding interactions with $NO_2$. The polymer also discriminates $NO_2$ over a range of analytes, such as $NH_3$, EtOH, MeOH, acetone, 2-nitrotoluene and water. We believe that this work may open up new design strategies for developing 1D organic polymer-based gas sensing materials with specific functional groups that effectively bind to a particular analyte.

**Acknowledgements** RRM thanks the Science and Engineering Research Board (SERB), India, for partially supporting this research through its Early Career Research Award Scheme (ECR/2018/002285) and IIT Dharwad for the seed grant. RG acknowledges the Council of Scientific and Industrial Research (CSIR), India, for supporting this work partially through Extramural Research Grant (22(0787)/19/EMR-II). We are grateful to the Sophisticated Central Instrumentation Facility (SCIF), IIT Dharwad, and its staff members for assisting us with the material characterizations. We also thank the University Scientific and Instruments Center (USIC), Karnataka University Dharwad; Instrumentation facility, Department of Chemistry, IIT Bombay for assisting with material characterization.

## Compliance with ethical standards

**Conflict of interest** The authors declare no competing interests.

**Publisher's note** Springer Nature remains neutral with regard to jurisdictional claims in published maps and institutional affiliations.

## References

1. Luttrell WE. Nitrogen dioxide. J Chem Heal Saf. 2014;21:28–30.
2. Manisalidis I, Stavropoulou E, Stavropoulos A, Bezirtzoglou E. Environmental and health impacts of air pollution: a review. Front Public Heal. 2020;8:1–13.
3. Kasuga, H Health effects of air pollution. *How to conquer air Pollut. a Japanese Exp*. 95–113 (1989).
4. Environmental Protection Agency (EPA). Nitrogen oxides (NOx), why and how they are controlled. *Epa-456/F-99-006R* 48 (1999).
5. Wöllenstein, J, Peter, C, Schmitt, K, Courbat, J & Briand, D D3.3 - Colorimetric gas sensors for the detection of am¬monia, nitrogen dioxide and carbon monoxide: Current Status and Research Trends. 135–135 (2020).
6. Schmitt K, Tarantik K, Pannek C, Sulz G, Wöllenstein J. Colorimetric gas sensing with enhanced sensitivity. Procedia Eng. 2016;168:1237–40.
7. Di Francia G, Alfano B, La Ferrara V. Conductometric gas nanosensors. J Sensors. 2009;2009:659275.
8. Pasierb P, Rekas M. Solid-state potentiometric gas sensors-current status and future trends. J Solid State Electrochem. 2009;13:3–25.
9. Wong YC, Ang BC, Haseeb ASMA, Baharuddin AA, Wong YH. Review—conducting polymers as chemiresistive gas sensing materials: a review. J Electrochem Soc 2020;167:037503.
10. Yu SH, Girma HG, Sim KM, Yoon S, Park JM, Kong H, et al. Polymer-based flexible $NO_x$ sensors with ppb-level detection at room temperature using breath-figure molding. Nanoscale. 2019;11:17709–17.
11. Yuvaraja S, Surya SG, Chernikova V, Vijjapu MT, Shekhah O, Bhatt PM, et al. Realization of an ultrasensitive and highly selective OFET $NO_2$ sensor: the synergistic combination of PDVT-10 polymer and porphyrin − MOF. ACS Appl Mater Interfaces 2020;12:18748–60.
12. Srinivasan P, Ezhilan M, Kulandaisamy AJ, Babu KJ, Rayappan JBB. Room temperature chemiresistive gas sensors: challenges and strategies—a mini review. J Mater Sci Mater Electron. 2019;30:15825–47.
13. Santra S, Hu G, Howe RCT, De Luca A, Ali SZ, Udrea F, et al. CMOS integration of inkjet-printed graphene for humidity sensing. Sci Rep. 2015;5:1–12.
14. Depari A, De Marcellis A, Ferri G, Flammini A. A complementary metal oxide semiconductor - Integrable conditioning circuit for resistive chemical sensor management. Meas Sci Technol. 2011;22:124001.
15. Fine GF, Cavanagh LM, Afonja A, Binions R. Metal oxide semiconductor gas sensors in environmental monitoring. Sensors. 2010;10:5469–502.
16. Kanan SM, El-Kadri OM, Abu-Yousef IA, Kanan MC. Semiconducting metal oxide based sensors for selective gas pollutant detection. Sensors. 2009;9:8158–96.
17. Ghosh R, Gardner JW, Guha PK. Air pollution monitoring using near room temperature resistive gas sensors: a review. IEEE Trans Electron Devices. 2019;66:3254–64.
18. Zhang Y, Jiang Y, Duan Z, Huang Q, Wu Y, Liu B, et al. Highly sensitive and selective NO2 sensor of alkalized V2CTx MXene driven by interlayer swelling. Sens Actuators B Chem. 2021;344:130150.
19. Liu B, Liu X, Yuan Z, Jiang Y, Su Y, Ma J, et al. A flexible $NO_2$ gas sensor based on polypyrrole/nitrogen-doped multiwall carbon nanotube operating at room temperature. Sensors Actuators B Chem. 2019;295:86–92.
20. Tang R, Shi Y, Hou Z, Wei L. Carbon nanotube-based chemiresistive sensors. Sensors. 2017;17:882.
21. Wang F, Gu H, Swager TM. Carbon nanotube/polythiophene chemiresistive sensors for chemical warfare agents. J Am Chem Soc. 2008;130:5392–3.

22. Fratoddi I, Venditti I, Cametti C, Russo MV. Chemiresistive polyaniline-based gas sensors: A mini review. Sensors Actuators B Chem. 2015;220:534–48.
23. Pandey S. Highly sensitive and selective chemiresistor gas/vapor sensors based on polyaniline nanocomposite: a comprehensive review. J Sci Adv Mater Devices. 2016;1:431–53.
24. dos Reis MAL, Thomazi F, del Nero J, Roman LS. Development of a chemiresistor sensor based on polymers-dye blend for detection of ethanol vapor. Sensors. 2010;10:2812–20.
25. Kwon OS, Park SJ, Yoon H, Jang J. Highly sensitive and selective chemiresistive sensors based on multidimensional polypyrrole nanotubes. Chem Commun. 2012;48:10526–8.
26. Wu D, Sedgwick AC, Gunnlaugsson T, Akkaya EU, Yoon J, James TD. Fluorescent chemosensors: The past, present and future. Chem Soc Rev. 2017;46:7105–23.
27. Liu B, Zhuang J, Wei G. Recent advances in the design of colorimetric sensors for environmental monitoring. Environ Sci Nano. 2020;7:2195–213.
28. Zhao Q, He Z, Jiang Y, Yuan Z, Wu H, Su C, et al. Enhanced acetone-sensing properties of PEI thin film by GO-NH2 functional groups modification at room temperature. Front Mater. 2019;5:1–5.
29. Bekyarova E, Davis M, Burch T, Itkis ME, Zhao B, Sunshine S, et al. Chemically functionalized single-walled carbon nanotubes as ammonia sensors. J Phys Chem B. 2004;108:19717–20.
30. Abel SB, Olejnik R, Rivarola CR, Slobodian P, Saha P, Acevedo DF, et al. Resistive sensors for organic vapors based on nanostructured and chemically modified polyanilines. IEEE Sens J. 2018;18:6510–6.
31. Cavallo P, Frontera E, Acevedo DF, Olejnik R, Slobodian P, Saha P, et al. Functionalized polyanilines made by nucleophilic addition reaction, applied in gas sensors field. Synth Met. 2016;215:127–33.
32. Yoon B, Choi SJ, Swager TM, Walsh GF. Flexible chemiresistive cyclohexanone sensors based on single-walled carbon nanotube-polymer composites. ACS Sens. 2021;6:3056–62.
33. Yoon B, Choi SJ, Swager TM, Walsh GF. Switchable single-walled carbon nanotube-polymer composites for $CO_2$ sensing. ACS Appl Mater Interfaces. 2018;10:33373–9.
34. Yang K, Yuan W, Hua Z, Tang Y, Yin F, Xia D. Triazine-based two-dimensional organic polymer for selective $NO_2$ sensing with excellent performance. ACS Appl Mater Interfaces. 2020;12:3919–27.
35. Tao LM, Niu F, Zhang D, Wang TM, Wang QH. Amorphous covalent triazine frameworks for high performance room temperature ammonia gas sensing. N J Chem 2014;38:2774–7.
36. Ko WC, Kim MS, Kwon YJ, Jeong J, Kim WR, Choi H, et al. Two-dimensional semiconducting covalent organic nanosheets for highly sensitive and stable NO2sensing under humid conditions. J Mater Chem A. 2020;8:19246–53.
37. Srinivasan P, Samanta S, Krishnakumar A, Rayappan JBB, Kailasam K. Insights into g-C3N4as a chemi-resistive gas sensor for VOCs and humidity-a review of the state of the art and recent advancements. J Mater Chem A. 2021;9:10612–51.
38. Sharma N, Sharma N, Srinivasan P, Kumar S, Balaguru Rayappan JB, Kailasam K. Heptazine based organic framework as a chemiresistive sensor for ammonia detection at room temperature. J Mater Chem A. 2018;6:18389–95.
39. Niu F, Shao ZW, Zhu JL, Tao LM, Ding Y. Structural evolution of imine-linked covalent organic frameworks and their NH3sensing performance. J Mater Chem C. 2021;9:8562–9.
40. Quinton C, Chi SH, Dumas-Verdes C, Audebert P, Clavier G, Perry JW, et al. Novel s-tetrazine-based dyes with enhanced two-photon absorption cross-section. J Mater Chem C. 2015;3:8351–7.
41. Joshi S, Raj KA, Rao MR, Ghosh R. An electronic biosensor based on semiconducting tetrazine polymer immobilizing matrix coated on rGO for carcinoembryonic antigen. Sci Rep. 2022;12:1–14.
42. Kulkarni S, Ghosh R. A simple approach for sensing and accurate prediction of multiple organic vapors by sensors based on CuO nanowires. Sensors Actuators. B Chem. 2021;335:129701.